Buletin Ilmiah Sarjana Teknik Elektro
Vol. 8, No. 6, December 2026, pp. 1776-1788
ISSN: 2685-9572, DOI: 10.12928/biste.v8i6.14995

Terrestrial Laser Scanning for Al-Mustansiriya School Archeological Site (Baghdad-Iraq)

Qamar Q. Muhammed [1], **Baydaa F. Hamad** [2], **Shiamaa D. Latef** [2], **Enas A. Zayed** [2], **Hussien Dulaimi** [1], **Huthaifa Al-Khazraji** [1], **Aws M. Abdullah** [2]
[1] University of Technology-Iraq, Baghdad, Iraq
[2] University of Baghdad, Baghdad, Iraq

ARTICLE INFORMATION

Article History:

Received 18 October 2025
Revised 26 November 2025
Accepted 20 November 2026

Keywords:

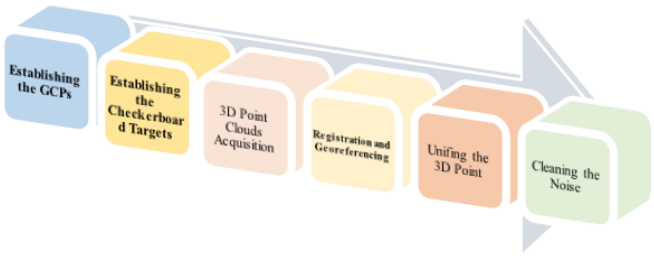
3D Point Cloud Registeration;
Archaeological Sites;
Terresterial Laser Scanning;
Al-Mustansiriya School

Corresponding Author:

Hussien Dulaimi,
University of Technology-Iraq
Baghdad, Iraq.
Email:
60179@uotechnology.edu.iq

This work is open access under a Creative Commons Attribution-Share Alike 4.0

ABSTRACT



This study demonstrates and evaluates a workflow for 3D heritage documentation using Terrestrial Laser Scanning (TLS) technology of archaeological and heritage buildings where the Al-Mustansiriya school building was selected as a case study. The practical side of the current study can be summarized in six stages. During the first step of the procedure, two Ground Control Points (GCPs) were set up in the inner courtyard of the school using the Leica GS15 GNSS device and processed through the Leica Geo Office software. In the second stage, based on the two GCPs, the Leica TS06+ Total Station device was employed to find the ground coordinates according to the UTM (Universal Transverse Mercator) coordinate system for a set of Checkerboard Targets installed on the walls of the school building. In the third phase, 3D point clouds were acquired by positioning the Leica ScanStation C10 TLS device at multiple locations throughout the site. In the fourth stage, the Leica Cyclone program was utilized to perform the registration process between point clouds registered in the TLS internal coordinate system and the global coordinate system UTM of the Checkerboard Targets such that the point clouds are computed according to the UTM coordinate system. The 3D point clouds were collected and unified into a unified single 3D point cloud during the fifth stage. Lastly, a cleaning and removal of noise and unwanted objects from final 3D point cloud has been carried out. The accuracy obtained based on the Mean Absolute Error MAE (0.5×10^(-3)m) from the current study is sufficient and suitable for many projects documenting archaeological and heritage buildings.

Document Citation:

Q. Q. Muhammed, B. F. Hamad, S. D. Latef, E. A. Zayed, H. Dulaimi, H. Al-Khazraji, and A. M. Abdullah, "Terrestrial Laser Scanning for Al-Mustansiriya School Archeological Site (Baghdad-Iraq)," *Buletin Ilmiah Sarjana Teknik Elektro*, vol. 8, no. 6, pp. 1776-1788, 2026, DOI: 10.12928/biste.v8i6.14995.

1. INTRODUCTION

Laser scanning systems can rapidly acquire highly detailed measurements of structures, often within a short time frame. They collect a vast number of distance and angular observations, which are subsequently converted into a dense three-dimensional point cloud consisting of millions of x,y,zx, y, zx,y,z coordinates that accurately represent the scanned object [1]. The first generations of Terrestrial Laser Scanning (TLS) devices appeared in the late 1990s and the early 2000s. Additional technical information about these early models can be found in [2]-[4]. A general overview of the specifications of TLS systems produced by well-known manufacturers such as Leica, Faro, Trimble, and Z+F is available in [5]. In the literature, discussions of the TLS technology are typically divided into two main areas. The first focuses on technical developments in the devices themselves—how they operate. The performance characteristics of the TLS depends on the measuring principle used either time-of-flight (ToF), or phase shift, as well as on such parameters as recording speed, the measuring range being measured and the accuracy of the individual laser points in space. Moreover, a second set of parameters affects fidelity of the resulting 3D point cloud (relative distance between scanner and target, colour and reflectivity of surface, horizontal and vertical angles of scanning, illumination in ambient and, additional contributing variables). Reference [6] provides a detailed discussion of the performance and efficiency of various TLS systems, comparative analyses of these parameters has been described in detail. In addition, the mathematical formulation and digital post-processing of TLS-derived 3D point clouds, especially the registration procedures are dealt with comprehensively in several specialized monographs (see references [7]-[10]). This method produces millions of highly accurate 3D points with extremely high point density, making it a valuable alternative to, or complement for, conventional topographic measurement techniques such as total stations and digital photogrammetry [11]. For the present investigation, the Leica Cyclone software suite was used to carry out the registration of TLS generated point clouds with real world coordinate systems, in this case UTM (Universal Transverse Mercator) reference frame. Further information on 3D coordinate systems and their principles can be found in standard photogrammetry and geodesy textbooks, such details are discussed in references [8][9]. From an implementation standpoint, the Leica Cyclone software applies a six-parameter 3D transformation model, which includes three parameters for translation and three for rotation [12].

Historic and heritage buildings (HHBs) play a crucial role in preserving cultural memory and identity. Highly valued by local communities and the broader public, the loss of these structures can erase meaningful links to history and tradition [13]-[15]. In this direction, TLS offers numerous benefits for cultural heritage documentation. In contrast to conventional techniques, which are often intrusive, labor-intensive, and susceptible to inaccuracies, TLS enables fast and highly accurate data capture while preserving the physical integrity of heritage sites. Therefore, several publications have been utilized the TLS technology for cultural heritage application and documentation including references [16]–[22].

This research deals with the use of TLS technology in the 3D photogrammetric and lasergrammetric documentation of archaeological/cultural heritage structure. The main problem, which is addressed in this work, is the absence of accurate 3D pictorial documentation (i.e. visual records) of the Iraqi's archaeological and heritage sites and constructions. This limitation hinders the country's ability to engage in Heritage Building Information Modeling (HBIM), a modern approach that plays a vital role in supporting the restoration, maintenance, and reconstruction of historic and cultural structures. The case study selected for this research focuses on the Al-Mustansiriya School in Baghdad, the importance of this school is evident because it is the first Islamic university, in addition to its nomination to join the World Heritage List in 2014 [23]. To address the above stated problems, the contribution of this study can be listed as follows:

- Experimental study on the application of TLS technology in the 3D photogrammetric documentation of archaeological buildings. The present study is an evaluation of the TLS application to the documentation of archaeological structures using AL-Mustansiriya School at Baghdad as an exemplary case study. The investigation further evaluates the flow efficiency in terms of accuracy, cost, and implementation time taken during the implementation process (hardware and software components utilized during the process).
- Preparation of the Basic Digital Requirements to Create the HBIM Model of the Archaeological Building. This stage focuses on preparing the fundamental digital data required to develop the HBIM model for the archaeological building under study. It involves conducting detailed 3D laser scanning to generate a precise 3D point cloud, which will later be utilized to construct three-dimensional models in standard CAD formats for representing the architectural and structural features of the building.

2. METHODS

2.1. Study Area (The Investigated Archaeological Site)

The Al-Mustansiriya School was an ancient educational institution which was established during the Abbasid era, in the city of Baghdad in 1233 AD by the Caliph Al-Mustansir Billah, and was a center of scientific and cultural in that era. The place of the school is located on the Rusafa sector of the city of Baghdad as shown in Figure 1. The school was constructed on an area of approximately 4,836 square meters, overlooking the eastern bank of the Tigris River near the Caliphate Palace. At the center of the school was a large courtyard featuring a fountain that housed the famous Al-Mustansiriya School clock, A remarkable feature of the Al-Mustansiriya School is its unique clock, which stands as a testament to the scientific advancement achieved by Arab scholars during that era. The clock was designed to announce prayer times throughout the day, reflecting the integration of science and daily life in the Abbasid period. The school itself consists of two floors containing around 100 rooms of varying sizes, in addition to several large halls used for teaching and academic gatherings. The first restoration of the Al-Mustansiriya School was undertaken in 1960, followed by a second phase of maintenance in 1973. In respect of its historical and architectural significance, in 2014, the school was included in the Tentative List of the World Heritage in the World Heritage Convention under the title of "The Historic Center of the City of Baghdad" [23].

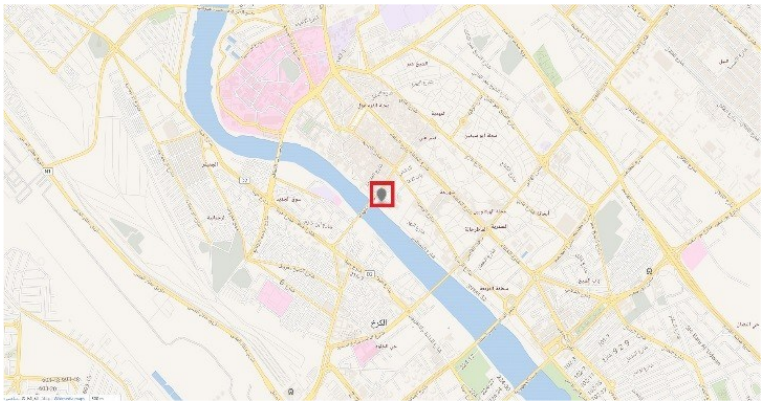


Figure 1. Site map of Al-Mustansiriya School, Baghdad, Iraq (Google Maps)

2.2. Tools and Software Packages

In the present research, the following tools were utilized: Leica GS015 GPS System (Figure 2) [24]. Leica TS06 Plus Total Station (Figure 3) [25]. Leica ScanStation C10 (Figure 4) [26]-[28]. MSI GL75 Laptop, equipped with an Intel Core i7-10750H CPU, Nvidia RTX 2070 GPU, 16 GB DDR4 2666 MHz RAM, and a 512 GB SSD main drive. CROWN CT44035 Digital Laser Measure and standard measuring tape.

Besides the tools, in the present study, the following software packages were employed: Leica Geo Office – used for GNSS data processing during both the initial and final stages. NGS OPUS Electronic Service [29]-[30] – utilized for the correction and refinement of GNSS data. Leica Cyclone – applied for processing the 3D point clouds captured by the Leica C10 TLS.



Figure 2. Main components of the GNSS System (Leica GS15)



Figure 3. The used Total Station (Leica-TS06-Plus)



Figure 4. Leica C10 TLS

2.3. The Framework

The overall work of this study (Figure 5) can be categorized into six parts, as follows:

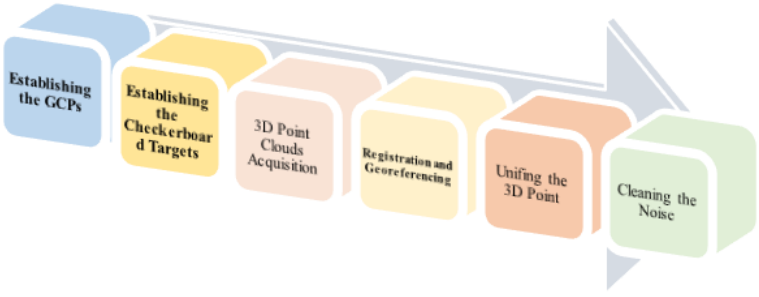


Figure 5. block diagram of the framework

2.3.1. Establishing Ground Control Points Using GNSS Techniques

The number of Ground Control Points (GCPs) were set to two and located inside the archaeological site using Geodesic Leica GS015, Geodesic Leica GS015 GNSS system, Leica Geo Office software and Opus Online Processing service. The procedure used was as follows:

- Determining the initial positions of the two selected points within the archaeological site.
- Setting up the Leica GS015 system, including both the base and rover units, on the designated GCP locations.
- Choosing the Static Mode for GNSS data acquisition to ensure high-precision measurements.
- Performing a preliminary processing of the GNSS data collected by the Leica Geo Office program.
- Uploading the base station data to the service on OPUS online for the differential correction and refinement.
- The base and rover datasets were processed in Leica Geo Office to get the accurate UTM coordinates of the two GCPs.

2.3.2. Establishing the Checkerboard Targets

The Leica TS06 Plus Total Station was employed with the referencing the previously established Ground Control Points (GCPs) to distribute a set of checkerboard targets across the façades selected for lasergrammetric investigation. These targets served as reference points to facilitate accurate registration and alignment of the 3D laser scans.

2.3.3. 3D Point Cloud Acquisition

The Terrestrial Laser Scanner (TLS) was positioned at multiple locations around the archaeological structure to capture a series of overlapping 3D point clouds. This approach ensured full coverage of the building façades and improved the accuracy of the subsequent registration and modeling processes.

2.3.4. Registration and Georeferencing

All 3D point clouds were registered and georeferenced to the UTM Zone 38N coordinate system for horizontal positioning and Mean Sea Level (MSL) for vertical elevation. The process employed a six-parameter 3D coordinate transformation, which includes three parameters for translation and three for rotation, to accurately align the TLS data within the real-world geospatial reference framework.

2.3.5. Unifying the 3D Point Clouds

The 3D point clouds on which the registration and georeferencing was performed were together integrated and unified on one point cloud.

2.3.6. Cleaning the Noise

At this point, noise and other undesired elements such as objects and people which are moving, and even scanning equipment itself were taken out from the final point cloud. This cleaning process ensured the generation of a refined dataset suitable for subsequent 3D modelling and processing, with the objective of converting the point cloud into accurate 3D CAD models.

3. RESULT AND DISCUSSION

3.1. Establishing the Ground Control Points using GNSS Techniques

First of all the position of two Ground Control Points (GCPs) were marked on the ground. Following this, two elements of this Leica GS015 system (the base and the rover) were placed on these nominated GCPs. The observation period and the spatial relationship of the first (control) and the second (measured) GCPs are illustrated in Figure 6 and Figure 7 respectively.

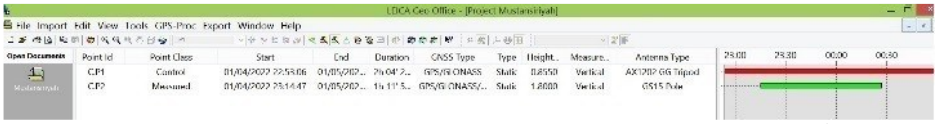


Figure 6. Observation time for the two Ground Control Points (1st GCP Control, 2nd GCP Measured)

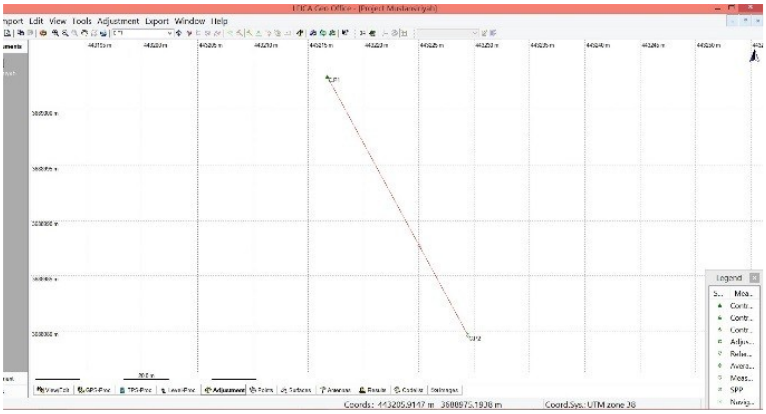


Figure 7. Spatial relationship between the two Ground Control Points (1st GCP Control, 2nd GCP Measured)

3.2. Establishing the Checkerboard Targets

The checkerboard targets that are crucial to the laser scanning procedure were attached to the walls at different points in the archaeological site, as shown in Figures 8 and 9. The two established GCPs were used as a basis to control and measured GCPs. The previously described GNSS techniques (Leica GS015 System, Leica Geo Office software and the NGS-OPUS service), the UTM coordinates and elevations of 28 checkerboard targets were determined using the Leica TS06 Plus Total Station. The measured data are presented in Table 1.



Figure 8. Checkerboard # 35



Figure 9. Checkerboard # 37

Table 1. Target Board (Checkerboard) with their UTM Coordinates

Target ID	Easting (Km)	Northing (Km)	Elevation (Km)
1	443.235	3688.996	0.035
2	443.218	3689.010	0.035
3	443.203	3689.021	0.035
4	443.189	3689.006	0.035
5	443.197	3688.991	0.035
6	443.219	3688.971	0.035
7	443.234	3688.961	0.036
8	443.250	3688.978	0.036
9	443.244	3689.003	0.035
10	443.276	3688.979	0.036
11	443.287	3688.971	0.036
12	443.245	3688.925	0.035
13	443.236	3688.929	0.036
14	443.163	3688.996	0.036
15	443.163	3689.005	0.035
16	443.194	3689.042	0.035
17	443.180	3689.026	0.036
18	443.241	3689.013	0.036
19	443.235	3689.015	0.038
20	443.222	3689.008	0.034
21	443.201	3689.019	0.034
22	443.187	3689.004	0.034
23	443.196	3688.982	0.034
24	443.206	3688.973	0.034
25	443.235	3688.960	0.034
26	443.250	3688.978	0.034
27	443.236	3688.996	0.034
28	443.216	3688.972	0.034

3.3. 3D Point Cloud Acquisition

The Leica ScanStation C10 was positioned at 15 different locations within the site of the Al-Mustansiriya School to ensure complete coverage of the structure, as illustrated in Figure 10 to Figure 15.

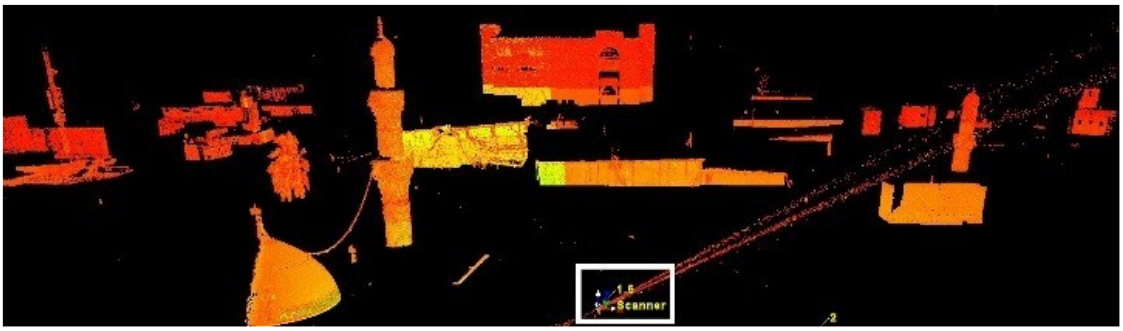


Figure 10. First position of the Leica ScanStation C10 (white box) placed on the roof of the northern part of the school building

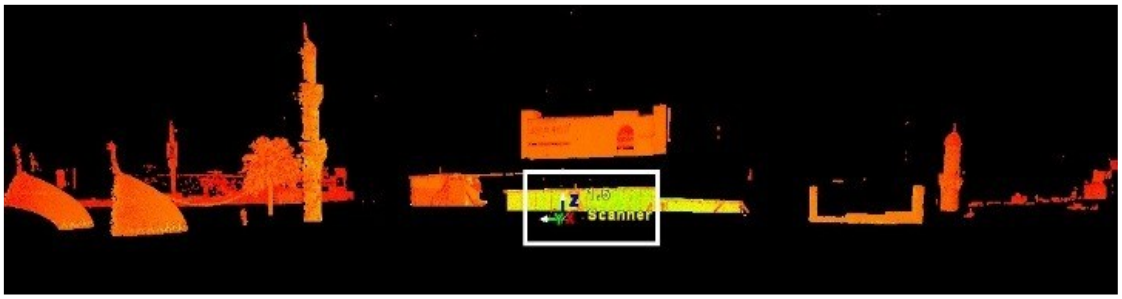


Figure 11. Second position of the Leica ScanStation C10 (white box) located on the east side of the roof of the school building

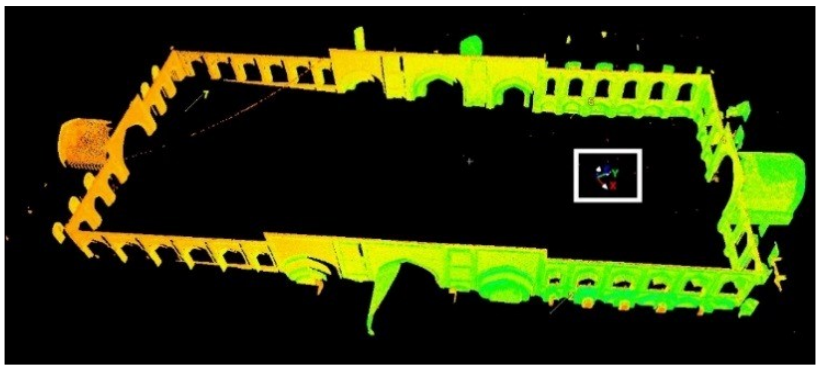


Figure 12. Ninth position of Leica ScanStation C10 (white box) in the inner courtyard at the school, facing the north iwan (Case 1)

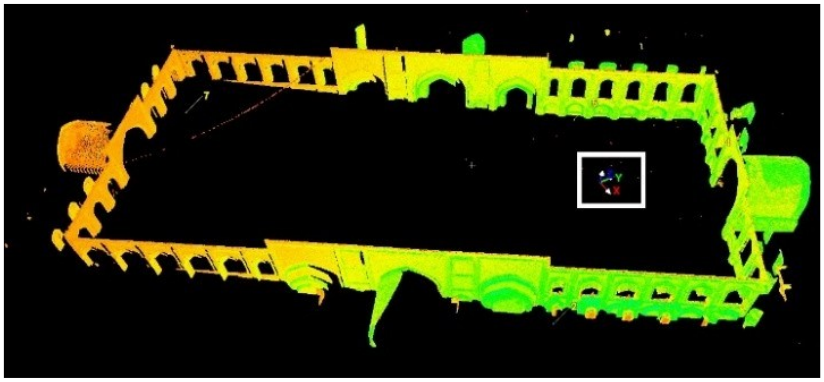


Figure 13. Ninth position of the Leica ScanStation (white box) of the school in the inner courtyard located at the Northern iwan (Case 1)

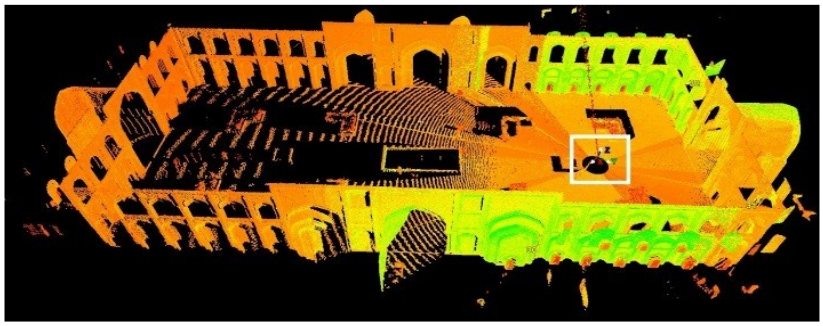


Figure 14. Tenth position of the Leica ScanStation C10 (white box) in the inner courtyard of the school, in the north iwan (Case 2)

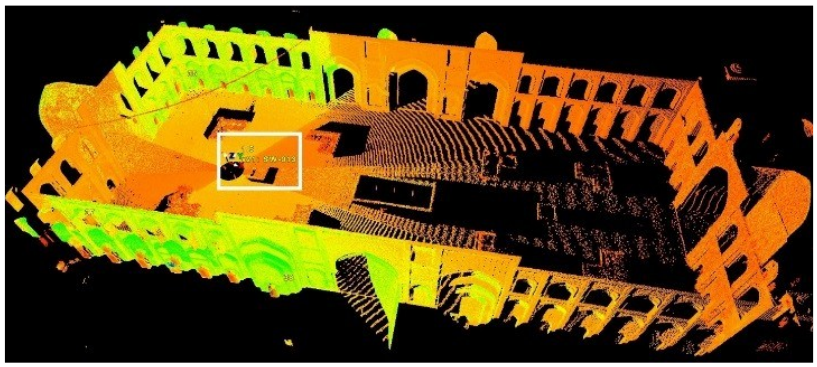


Figure 15. Twelfth position of the Leica ScanStation C10 (white box), was in the inner courtyard of the school in the southern iwan (Case 2)

3.4. Registration and Georeferencing

Based on the 3D conformal transformation (six-parameter model) applied using the Leica Cyclone software, the numerical results of the registration process were obtained and are presented in Table 2.

Table 2. The registration results

	S	Position of Scanner Station (S#)	Recognized Checkerboard Target	Error (m)	Error Vector (m)
			1	0.002	(-0.002,0.000 ,0.000)
		The central of the school's inner courtyard for observing some checkerboard targets (figure 31)	2	0.002	(0.000, -0.002, -0.001)
			3	0.003	(0.002,-0.003 ,0.001)
			6	0.004	(0.001, 0.004,0.000)
			8	0.002	(-0.002,0.001 ,0.001)
1	S1	Translation Transformations Parameters	Easting-X (Km)	Northing-Y (Km)	Elevation-Z (Km)
			443.219	3688.992	0.035
		Rotation Transformations Parameters	X-Axis (deg.)	Y-Axis (deg.)	Z-Axis(deg.)
			0.0000	0.0000	128.2760
		the south side of the primary gate of the school (figure 21)	15	0.009	(0.005,-0.005 ,-0.004)
			17	0.007	(-0.004,0.006 ,0.000)
			18	0.005	(-0.001,-0.001,-0.005)
2	S10	Translation Transformations Parameters	Easting-X (Km)	Northing-Y (Km)	Elevation-Z (Km)
			443.283	3688.970	0.036
		Rotation Transformations Parameters	X-Axis (deg.)	Y-Axis(deg.)	Z-Axis(deg.)
			0.0000	0.0000	44.309
		In front of the southern outer iwan (figure 22)	23	0.005	(0.001,0.005 ,0.000)
			22	0.005	(0.004,0.002 ,-0.002)
			21	0.009	(-0.005,-0.007,-0.001)
3	S11	Translation Transformations Parameters	Easting-X (Km)	Northing-Y (Km)	Elevation-Z (Km)
			443.178	3689.023	0.036
		Rotation Transformations Parameters	X-Axis (deg.)	Y-Axis(deg.)	Z-Axis(deg.)
			0.0000	0.0000	88.693
		In front of the primary Gate (figure 23)	25	0.002	(0.002,-0.001 ,0.000)
			24	0.002	(-0.002,0.001 ,0.000)
4	S12	Translation Transformations Parameters	Easting-X (Km)	Northing-Y (Km)	Elevation-Z (Km)
			443.238	3689.012	0.037
		Rotation Transformations Parameters	X-Axis (deg.)	Y-Axis(deg.)	Z-Axis(deg.)
			0.0000	0.0000	69.478
		the inner courtyard of the school _ the northern iwan (figure 26)	2	0.006	(-0.002,0.004 ,0.002)
			4	0.003	(0.001,-0.002 ,0.001)
			5	0.011	(0.011,-0.001 ,0.000)
			7	0.032	(-0.004,-0.012,-0.030)
5	S2	Translation Transformations Parameters	Easting-X (Km)	Northing-Y (Km)	Elevation-Z (Km)
			443.202	3689.001	0.036
		Rotation Transformations Parameters	X-Axis (deg.)	Y-Axis(deg.)	Z-Axis(deg.)
			0.0000	0.0000	80.875
		the central of the school's inner courtyard (figure 30)	30	0.002	(-0.001,-0.001,0.001)
			31	0.002	(0.001,0.001 ,0.001)
6	S20	Translation Transformations Parameters	Easting-X (Km)	Northing-Y (Km)	Elevation-Z (Km)
			443.219	3688.991	0.034
		Rotation Transformations Parameters	X-Axis (deg.)	Y-Axis(deg.)	Z-Axis(deg.)
			0.0000	0.0000	-33.175
		inner courtyard of the school_ the southern iwan_2 (figure 29)	35	0.002	(0.000,-0.002 ,0.001)
			37	0.003	(0.001,-0.002 ,-0.001)
			38	0.003	(-0.002,0.001 ,0.001)
7	S21	Translation Transformations Parameters	Easting-X (Km)	Northing-Y (Km)	Elevation-Z (Km)
			443.233	3688.977	0.034
		Rotation Transformations Parameters	X-Axis (deg.)	Y-Axis(deg.)	Z-Axis(deg.)
			0.0000	0.0000	119.545
		the internal courtyard of the school _ the northern iwan _2 (figure 27)	30	0.001	(-0.001,0.000 ,-0.001)
			31	0.001	(-0.011,-0.001,0.000)
8	S23		32	0.002	(0.001,0.001 ,0.000)
		Translation Transformations	Easting-X	Northing-Y	Elevation-Z

S		Position of Scanner Station (S#)	Recognized Checkerboard Target	Error (m)	Error Vector (m)
		Parameters	(Km)	(Km)	(Km)
			443.204	3689.004	0.034
		Rotation Transformations Parameters	X-Axis (deg.)	Y-Axis(deg.)	Z-Axis(deg.)
			0.0000	0.0000	6.858
		the middle of mosque hall (figure 25)	33	0.001	(0.000,0.000 ,-0.001)
			34	0.001	(-0.001,0.000 ,0.000)
			39	0.001	(0.000,0.000 ,0.001)
9	S24	Translation Transformations Parameters	Easting-X (Km)	Northing-Y (Km)	Elevation-Z (Km)
			443.207	3688.978	0.034
		Rotation Transformations Parameters	X-Axis (deg.)	Y-Axis(deg.)	Z-Axis(deg.)
			0.0000	0.0000	143.422
		inner courtyard of the school_ the southern iwan_1 (figure 28)	1	0.010	(-0.005,-0.008,0.001)
			3	0.004	(0.002,-0.002 ,0.001)
			6	0.003	(0.003,0.001 ,0.000)
10	S3		7	0.003	(-0.001,0.002 ,-0.001)
		Translation Transformations Parameters	Easting-X (Km)	Northing-Y (Km)	Elevation-Z (Km)
			443.233	3688.977	0.036
		Rotation Transformations Parameters	X-Axis (deg.)	Y-Axis(deg.)	Z-Axis(deg.)
			0.0000	0.0000	-83.879
		the northern rooftop of the school building (figure 18)	2	0.006	(0.004,0.005 ,0.000)
			7	0.003	(0.000,0.003 ,0.001)
			8	0.004	(-0.003,0.002 ,-0.001)
11	S4	Translation Transformations Parameters	Easting-X (Km)	Northing-Y (Km)	Elevation-Z (Km)
			443.184	3689.004	0.047
		Rotation Transformations Parameters	X-Axis (deg.)	Y-Axis(deg.)	Z-Axis(deg.)
			0.0000	0.0000	-31.890
		the western roof of the school building (figure 32)	3	0.010	(-0.009,-0.002,0.008)
			4	0.008	(0.007,0.005 ,-0.006)
12	S5	Translation Transformations Parameters	Easting-X (Km)	Northing-Y (Km)	Elevation-Z (Km)
			443.247	3688.965	0.047
		Rotation Transformations Parameters	X-Axis (deg.)	Y-Axis(deg.)	Z-Axis(deg.)
			0.0000	0.0000	-84.916
		the eastern roof of the school building (figure 19)	5	0.01	(0.005,-0.004 ,0.007)
			7	0.007	(-0.005,0.004 ,-0.002)
13	S6	Translation Transformations Parameters	Easting-X (Km)	Northing-Y (Km)	Elevation-Z (Km)
			443.205	3689.024	0.047
		Rotation Transformations Parameters	X-Axis (deg.)	Y-Axis(deg.)	Z-Axis(deg.)
			0.0000	0.0000	84.810
		Behind the school, inside the outer wall (figure 24)	20	0.003	(0.002,-0.002 ,0.000)
			19	0.005	(-0.002,0.002 ,0.004)
14	S8	Translation Transformations Parameters	Easting-X (Km)	Northing-Y (Km)	Elevation-Z (Km)
			443.182	3688.979	0.035
		Rotation Transformations Parameters	X-Axis (deg.)	Y-Axis(deg.)	Z-Axis(deg.)
			0.0000	0.0000	-133.677
		on the northern side of the school building (figure 20)	15	0.011	(0.003,-0.002 ,-0.011)
			16	0.004	(-0.003,0.002 ,-0.001)
15	S9	Translation Transformations Parameters	Easting-X (Km)	Northing-Y (Km)	Elevation-Z (Km)
			443.267	3688.984	0.036
		Rotation Transformations Parameters	X-Axis (deg.)	Y-Axis(deg.)	Z-Axis(deg.)
			0.0000	0.0000	-52.089
Mean Absolute Error (m)					**0.0049**

3.5. Unifying and Cleaning

A single 3D point cloud that represents the whole archaeological site was created by unification of all the point clouds of individual registration. The Fence, Region Grow, and other tools that come with the Leica Cyclone software was used to create the end result of the cleaned and refined point cloud of the site. Several

visualizations of this unified, registered, and cleaned 3D point cloud captured from different viewing angles are presented in Figure 16 to Figure 18.

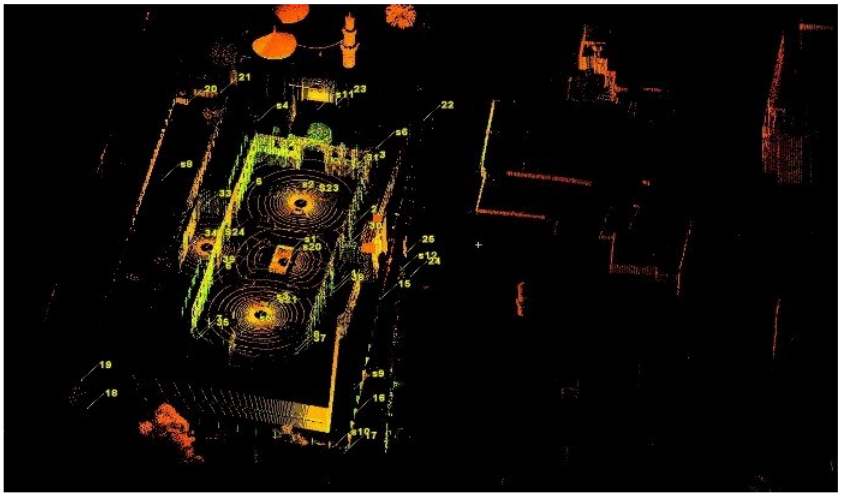


Figure 16. View of the unified 3D point cloud of the site, as seen from the south-to-north direction

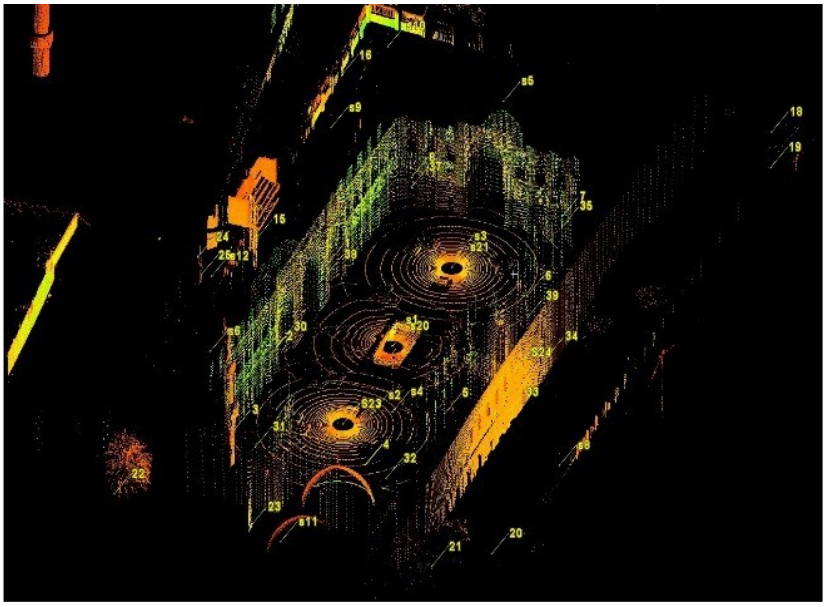


Figure 17. View of the unified 3D point cloud of the site, as seen from the southeast-to-northwest direction



Figure 18. View of the unified 3D point cloud of the site, as seen from the east-to-west direction

4. CONCLUSIONS

The conclusion of this study can be stated as follows:

- The resulting 3D point cloud of the archaeological site serves as a foundational database for the precise surveying stage in the development of Heritage Building Information Modeling (HBIM) for the investigated site.
- Due to high cost for using the TLS (about 300$ per one hour), the scanning resolution has not been selected to the highest option. With taking in consideration that, the scanning rate of the used TLS is only 50000 point per second (this scanning rate is very slow compared with 1000000 points per second or even 2000000 points per second for the latest versions of Leica TLS devices). Certainly, using such as device with highest resolution option will significantly increase the accuracy of the results but this option requires massive budget.
- Only two ground control points were employed by utilizing survey mode GNSS approaches which was satisfactory for positioning checkerboard targets with a tolerance of 0.1 m to 0.005 m or acceptable for projects over small areas. When the tolerance required is below 5 mm, or when the project covers large area, it is recommended that number of ground control points should be increased and the gap between the points should be increased.
- Observing the checkerboard targets using a terrestrial laser scanner (TLS) is a must for finishing the laser scanning operation of the building. In the current study, each of the TLS positions led to identification of two to three targets. This configuration is considered adequate in cases where accuracy and level of detail requirement are moderate. For projects that require greater accuracy and detail an increase in the number of targets in the checkerboard observed by the TLS should be made before beginning the laser scanning process.

REFERENCES

[1] A. E. Oseni, O. K. Ajani, A. J. Adewale, O. O. Ayodeji, and T. O. Desalu, "3D modelling of structures using terrestrial laser scanning technique," *Int. J. Adv. Eng., Manage. Sci. (IJAEMS)*, vol. 5, no. 7, pp. 316–331, 2020, https://doi.org/10.22161/ijaems.67.4.

[2] M. Akin, İ. Dinçer, A. Ö. Ok, A. Orhan, M. K. Akin, and T. Topal, "Assessment of the effectiveness of a rockfall ditch through 3-D probabilistic rockfall simulations and automated image processing," *Eng. Geol.*, vol. 283, p. 106001, 2021, https://doi.org/10.1016/j.enggeo.2021.106001.

[3] M. Sabzali and L. Pilgrim, "A comprehensive review of mathematical error characterization and mitigation strategies in terrestrial laser scanning," *Remote Sensing*, vol. 17, no. 14, p. 2528, 2025, https://doi.org/10.3390/rs17142528.

[4] A. Aryan, F. Bosché, and P. Tang, "Planning for terrestrial laser scanning in construction: A review," *Autom. Constr.*, vol. 125, p. 103551, 2021, https://doi.org/10.1016/j.autcon.2021.103551.

[5] J. Shan and C. K. Toth, *Topographic Laser Ranging and Scanning: Principles and Processing*. Boca Raton, FL, USA: CRC Press, 2018, https://doi.org/10.1201/9781315154381.

[6] S. Someya, "Particle-based temperature measurement coupled with velocity measurement," *Meas. Sci. Technol.*, vol. 32, p. 042001, 2021, https://doi.org/10.1088/1361-6501/abc0b0.

[7] S. Rani, K. Lakhwani, and S. Kumar, "Three dimensional objects recognition & pattern recognition technique; related challenges: A review," *Multimed. Tools Appl.*, vol. 81, pp. 17303–17346, 2022, https://doi.org/10.1007/s11042-022-12412-2.

[8] N. Pfeifer, G. Mandlburger, and P. Glira, "Laserscanning," In *Photogrammetrie und Fernerkundung: Handbuch der Geodäsie, herausgegeben von Willi Freeden und Reiner Rummel*, pp. 431-481, 2017, https://doi.org/10.1007/978-3-662-47094-7_44.

[9] T. Luhmann, S. Robson, S. Kyle, and J. Boehm, *Close-Range Photogrammetry and 3D Imaging*, 3rd ed. Berlin, Germany: De Gruyter, 2019, https://doi.org/10.1515/9783110607253.

[10] K. D. Rocha *et al*., "Crown-level structure and fuel load characterization from airborne and terrestrial laser scanning in a longleaf pine (Pinus palustris Mill.) forest ecosystem," *Remote Sensing*, vol. 15, no. 4, p. 1002, 2023, https://doi.org/10.3390/rs15041002.

[11] W. Wang, W. Zhao, L. Huang, V. Vimarlund, and Z. Wang, "Applications of terrestrial laser scanning for tunnels: A review," *J. Traffic Transp. Eng. (Engl. Ed.)*, vol. 1, no. 5, pp. 325–337, 2014, https://doi.org/10.1016/S2095-7564(15)30279-8.

[12] F. Schill, C. Holst, D. Wujanz, J. Hartmann, and J. A. Paffenholz, "Intensity-based stochastic model of terrestrial laser scanners: Methodological workflow, empirical derivation and practical benefit," *ISPRS Open Journal of Photogrammetry and Remote Sensing*, vol. 15, p. 100079, 2025, https://doi.org/10.1016/j.ophoto.2024.100079.

[13] P. Zdrenghea, C. B. Vîlceanu, S. Herban, and A. Alionescu, "Using the laser scanning for conservation of cultural heritage buildings," In *AIP Conference Proceedings*, vol. 3094, no. 1, p. 420008, 2024, https://doi.org/10.1063/5.0213285.

[14] D. Hawkes *et al.*, "Conservation of architectural heritage," *Adv. Sci., Technol. Innov.*, vol. 3, pp. 30–32, 2019, https://doi.org/10.1007/978-3-030-10871-7.

[15] E. Stylianidis, *Photogrammetric Survey for the Recording and Documentation of Historic Buildings*. Cham, Switzerland: Springer, 2020, https://doi.org/10.1007/978-3-030-47310-5.
[16] M. Ioannides and Q. Ewald, "3D research challenges in cultural heritage," *Lect. Notes Comput. Sci.*, vol. 8355, p. 151, 2014, https://doi.org/10.1007/978-3-662-44630-0.
[17] A. Llabani and F. Abazaj, "3D documentation of cultural heritage using terrestrial laser scanning," *J. Appl. Eng. Sci.*, vol. 22, no. 2, pp. 267–271, 2024, https://doi.org/10.5937/jaes0-50414.
[18] M. Ioannides *et al.*, "Digital Heritage: Progress in Cultural Heritage. Documentation, Preservation, and Protection (EuroMed 2016)," In *International Euro-Mediterranean Conference on Digital Heritage, EuroMed*, 2016, https://doi.org/10.1007/978-3-319-13695-0.
[19] F. Soler, F. J. Melero, and M. V. Luzón, "A complete 3D information system for cultural heritage documentation," *J. Cult. Herit.*, vol. 23, pp. 49–57, 2017, https://doi.org/10.1016/j.culher.2016.09.008.
[20] F. Remondino and A. Rizzi, "Reality-based 3D documentation of natural and cultural heritage sites—techniques, problems, and examples," *Appl. Geomat.*, vol. 2, no. 3, pp. 85–100, 2010, https://doi.org/10.1007/s12518-010-0025-x.
[21] E. Stylianidis, K. Evangelidis, R. Vital, P. Dafiotis, and S. Sylaiou, "3D documentation and visualization of cultural heritage buildings through the application of geospatial technologies," *Heritage*, vol. 5, no. 4, pp. 2818–2832, 2022, https://doi.org/10.3390/heritage5040146.
[22] J. Pilger, *Freedom Next Time*. Random House, 2007, https://books.google.co.id/books?hl=id&lr=&id=z0QD58GtDTYC.
[23] M. N. i. K. Al-Mukhtar, "Means of managing financial in the Abbasid state," *J. Tikrit Univ. Humanit.*, vol. 29, pp. 301–331, 2022, https://doi.org/10.25130/jtuh.29.12.2.2022.14.
[24] Ö. Yıldırım, "Regularised computation of 3D coordinates and orthometric heights for northern Cyprus: New network computations for northern Cyprus," *Boll. Geofis. Teor. Appl.*, vol. 61, 2020, https://doi.org/10.4430/bgta0308.
[25] A. Vivat, M. Fys, V. Litynskyi, T. Korliatovych, and I. Pokotylo, "The spatial determination of the point position by linear measurements," In *International Conference of Young Professionals <GeoTerrace-2020>*, vol. 2020, no. 1, pp. 1-5, 2020, https://doi.org/10.3997/2214-4609.20205723.
[26] A. Masiero, F. Fissore, A. Guarnieri, M. Piragnolo, and A. Vettore, "Comparison of low cost photogrammetric survey with TLS and Leica Pegasus backpack 3D models," *Int. Arch. Photogramm., Remote Sens. Spatial Inf. Sci.*, vol. 42, pp. 147–153, 2017, https://doi.org/10.5194/isprs-archives-XLII-2-W8-147-2017.
[27] D. A. Gura, D. A. Bespyatchuk, S. V. Samarin, N. M. Kiryunikova, and E. D. Lesovaya, "Technology of three-dimensional laser scanning as a tool to provide safety for sport facilities," *Nanotechnol. Constr.*, vol. 13, no. 4, pp. 259–263, 2021, https://doi.org/10.15828/2075-8545-2021-13-4-259-263.
[28] J. M. Vilbig, V. Sagan, and C. Bodine, "Archaeological surveying with airborne LiDAR and UAV photogrammetry: A comparative analysis at Cahokia Mounds," *Journal of Archaeological Science: Reports*, vol. 33, p. 102509, 2020, https://doi.org/10.1016/j.jasrep.2020.102509.
[29] D. T. Gillins, D. Kerr, and B. Weaver, "Evaluation of the online positioning user service for processing static GPS surveys: OPUS-Projects, OPUS-S, OPUS-Net, and OPUS-RS," *J. Surv. Eng.*, vol. 145, no. 3, p. 05019002, 2019, https://doi.org/10.1061/(ASCE)SU.1943-5428.0000280.
[30] D. T. Gillins and M. J. Eddy, "Comparison of GPS height modernization surveys using OPUS-Projects and following NGS-58 guidelines," *J. Surv. Eng.*, vol. 143, no. 1, p. 05016007, 2017, https://doi.org/10.1061/(ASCE)SU.1943-5428.0000196.